



Observation of the semileptonic decay $B^+ \rightarrow p\bar{p}\mu^+\nu_\mu$

LHCb collaboration[†]

Abstract

The Cabibbo-suppressed semileptonic decay $B^+ \rightarrow p\bar{p}\mu^+\nu_\mu$ is observed for the first time. The differential branching fraction is measured as a function of the $p\bar{p}$ invariant mass, using the mode $B^+ \rightarrow (J/\psi \rightarrow \mu^+\mu^-)K^+$ for normalisation. The total branching fraction is also measured to be

$$\mathcal{B}(B^+ \rightarrow p\bar{p}\mu^+\nu_\mu) = (5.27_{-0.24}^{+0.23} \pm 0.21 \pm 0.15) \times 10^{-6},$$

where the first uncertainty is statistical, the second systematic and the third is from the uncertainty on the normalisation branching fraction.

For submission to JHEP

© 2019 CERN for the benefit of the LHCb collaboration. CC-BY-4.0 licence.

[†]Authors are listed at the end of this paper.

1 Introduction

Studies of semileptonic B meson decays have recently generated interest due to a number of anomalous results. Measurements of the observables $R(D)$ and $R(D^*)$ [1–6] have shown hints of lepton nonuniversality with a combined significance of over 3σ [7]. To probe the flavour structure of any possible new physics contributions to these results, it is desirable to make analogous measurements for decays involving different quark transitions, for example $b \rightarrow u$. To that end, the mode $B^+ \rightarrow p\bar{p}l^+\nu_l$ is promising experimentally, particularly when performing the measurement at a hadron collider, as the requirement of two protons in the final state should significantly reduce combinatorial background. Semileptonic decays of B mesons to a final state containing multiple baryons are as yet unobserved, although the Belle collaboration has found evidence for $B^+ \rightarrow p\bar{p}e^+\nu_e$ with 3.2σ significance [8]. They measured the branching fraction to be $(8.2^{+3.7}_{-3.2} \pm 0.6) \times 10^{-6}$.

A theoretical model of $B^+ \rightarrow p\bar{p}\mu^+\nu_\mu$ has been constructed with perturbative QCD (pQCD) [9]. This model is based on studies of several similar fully hadronic $B \rightarrow Y\bar{Y}'X$ decays where Y represents a baryon and X one or more mesons. By fitting the angular distributions and decay rates of the hadronic modes [10, 11] the authors of this paper estimate the total branching fraction and the differential decay rate of $B^+ \rightarrow p\bar{p}\mu^+\nu_\mu$. However, the predicted branching fraction is two orders of magnitude larger than the Belle measurement.

The measurements of the fully hadronic modes show some features that merit further investigation. It is surprising that the branching fraction of $B^0 \rightarrow p\bar{p}$ is two orders of magnitude smaller than that of the almost equivalent decay $B^0 \rightarrow p\bar{p}\pi^+\pi^-$ [12, 13]. Furthermore, the invariant mass distributions of the dibaryon pair in $B \rightarrow Y\bar{Y}'X$ decays show a characteristic shape that peaks at low values [14–16]. Understanding the dynamics that leads to such features is difficult in fully hadronic decays, due to the interaction of the two baryons and the extra hadrons. It is therefore desirable to study semileptonic decays, such as $B^+ \rightarrow p\bar{p}\mu^+\nu_\mu$, where such final state interactions are absent.

In this paper, the first observation of the decay $B^+ \rightarrow p\bar{p}\mu^+\nu_\mu$ is presented. As the dynamics of the transition are not known, the branching fraction is measured in bins of $p\bar{p}$ invariant mass. These bins are then summed to obtain a measurement of the total branching fraction. The measurement is made relative to the normalisation mode $B^+ \rightarrow J/\psi K^+$, with $J/\psi \rightarrow \mu^+\mu^-$. The branching fraction within a bin i is

$$\frac{d\mathcal{B}(B^+ \rightarrow p\bar{p}\mu^+\nu_\mu)_i}{dm(p\bar{p})} = \frac{N(B^+ \rightarrow p\bar{p}\mu^+\nu_\mu)_i}{N(B^+ \rightarrow (J/\psi \rightarrow \mu^+\mu^-)K^+)} \times \frac{\epsilon(B^+ \rightarrow (J/\psi \rightarrow \mu^+\mu^-)K^+)}{\epsilon(B^+ \rightarrow p\bar{p}\mu^+\nu_\mu)_i} \times \mathcal{B}(B^+ \rightarrow (J/\psi \rightarrow \mu^+\mu^-)K^+), \quad (1)$$

where $N(B^+ \rightarrow p\bar{p}\mu^+\nu_\mu)_i$ is the yield of $B^+ \rightarrow p\bar{p}\mu^+\nu_\mu$ candidates in bin i , $N(B^+ \rightarrow (J/\psi \rightarrow \mu^+\mu^-)K^+)$ is the total yield of $B^+ \rightarrow J/\psi K^+$ candidates and ϵ represents the detector acceptance and reconstruction and selection efficiencies of the two modes. The branching fractions of $B^+ \rightarrow J/\psi K^+$ and $J/\psi \rightarrow \mu^+\mu^-$ decays are taken from Ref. [13].

The signal yields are extracted from fits to a variable called the corrected mass. It is defined by [17]

$$m_{corr} = |p'_T| + \sqrt{|p'_T|^2 + m_{vis}^2}, \quad (2)$$

40 where $|p'_T|$ is defined as the magnitude of the reconstructed $p\bar{p}\mu^+$ candidate momentum
41 transverse to the B flight direction and m_{vis}^2 is the square of the invariant mass of the
42 candidate.

43 The data sample for this study is that collected by the LHCb detector in proton-proton
44 collisions in 2011, 2012 and 2016. This corresponds to integrated luminosities of 1.0 fb^{-1} ,
45 2.0 fb^{-1} and 1.9 fb^{-1} at centre-of-mass energies of 7 TeV, 8 TeV and 13 TeV respectively.
46 The 2011 and 2012 datasets are treated together and collectively referred to by the
47 sobriquet Run 1. Charge conjugate processes are implied throughout this document.

48 2 Detector and simulation

49 The LHCb detector [18, 19] is a single-arm forward spectrometer covering the
50 pseudorapidity range $2 < \eta < 5$, designed for the study of particles containing b or
51 c quarks. The detector includes a high-precision tracking system consisting of a silicon-
52 strip vertex detector surrounding the pp interaction region [20], a large-area silicon-strip
53 detector located upstream of a dipole magnet with a bending power of about 4 Tm, and
54 three stations of silicon-strip detectors and straw drift tubes [21, 22] placed downstream
55 of the magnet. The tracking system provides a measurement of the momentum, p , of
56 charged particles with a relative uncertainty that varies from 0.5% at low momentum
57 to 1.0% at 200 GeV/ c . The minimum distance of a track to a primary vertex (PV), the
58 impact parameter (IP), is measured with a resolution of $(15 + 29/p_T)\text{ }\mu\text{m}$, where p_T is
59 the component of the momentum transverse to the beam, in GeV/ c . Different types of
60 charged hadrons are distinguished using information from two ring-imaging Cherenkov
61 (RICH) detectors [23]. Photons, electrons and hadrons are identified by a calorimeter
62 system consisting of scintillating-pad and preshower detectors, an electromagnetic and a
63 hadronic calorimeter. Muons are identified by a system composed of alternating layers of
64 iron and multiwire proportional chambers [24].

65 The online event selection is performed by a trigger [25], which consists of a hardware
66 stage that performs some basic selection, followed by a software stage, which applies a
67 full event reconstruction. At the first level, a track consistent with being a muon with
68 significant p_T is required to be present in the event. Subsequently in the software stage,
69 two tracks are required to form a secondary vertex with significant displacement from a
70 pp interaction vertex. A multivariate algorithm [26] is used to identify vertices that are
71 consistent with the decay of a b hadron.

72 Simulation is used to determine the efficiency of the signal mode and estimate the shapes
73 of the signal and several background modes in the fit. In the simulation, pp collisions are
74 generated using PYTHIA [27] with a specific LHCb configuration [28]. Decays of unstable
75 particles are described by EVTGEN [29], in which final-state radiation is generated using
76 PHOTOS [30]. The interaction of the generated particles with the detector, and its response,
77 are implemented using the GEANT4 toolkit [31], as described in Ref. [32]. The generated
78 B meson p and p_T spectra are corrected to match the data distributions. A boosted
79 decision tree (BDT) reweighter [33] is trained on samples of $B^+ \rightarrow J/\psi K^+$ data and
80 simulation, independent of those used for the normalisation of the branching fraction.
81 This is then used to correct all of the simulation used in the analysis.

3 Selection

Signal candidates are constructed from three tracks which are required to be of good quality and have a large IP with respect to any PV. The tracks must also have particle identification criteria consistent with their particle hypothesis. The requirement for positive proton identification in turn enforces a minimum p of 18 GeV/ c such that they are above the threshold for radiating in the RICH. Similarly, the muons must have p above 3 GeV/ c to propagate through the muon stations. All the daughter tracks must have p_T larger than 1.5 GeV/ c . Finally, the three tracks must form a good quality vertex significantly displaced from the PV with which the candidate is associated. The muon from the signal candidate must be that which fired the hardware trigger and then the reconstructed candidate itself must be consistent with the object that fired the software trigger. Potential decays of η_c , J/ψ and $\psi(2S)$ to $p\bar{p}$ are vetoed with cuts on the $p\bar{p}$ invariant mass of ± 50 MeV around the respective nominal masses.

The selection of the $B^+ \rightarrow (J/\psi \rightarrow \mu^+\mu^-)K^+$ normalisation mode is aligned with that of the signal to reduce systematic uncertainties. The cuts on the signal protons are applied to the K^+ and the muon of opposite sign (μ^-), with the exception of the particle identification criteria. The remaining muon has the signal muon selection applied to it.

Further selection is used to reduce several sources of backgrounds relative to the signal. The largest contribution comes from a melange of partially reconstructed decays producing two protons and a muon in the final state. It is expected that the largest among these would originate in $b \rightarrow c$ transitions. The most pernicious is $B \rightarrow \bar{A}_c^- p \mu^+ \nu_\mu X$, where X represents any number of charged or neutral pions (including none), where the \bar{A}_c^- decays to a final state including one proton. The other major background arises from $B \rightarrow p\bar{p}DX$ decays, where the D meson may be of any variety (D^0 , D^+ , D^{*+} etc.) but ultimately decays to a final state with a muon. A similar decay of $B \rightarrow p\bar{A}_c^- X$ with the \bar{A}_c^- decaying semileptonically is comparatively small, as the semileptonic branching fraction is dominated by $\bar{A}_c^- \rightarrow \Lambda l^- \bar{\nu}_l$ decays and the Λ flies a sufficient distance within the detector before decaying such that the resulting proton is not associated with the B decay vertex. Another source of partially reconstructed background is formed of $B \rightarrow p\bar{p}\mu^+\nu_\mu X$ decays, where X denotes one or more charged or neutral pions. These decays may proceed with intermediate N^* or Δ resonances and could naively be expected to have similar branching fractions to the signal.

If any of these partially reconstructed decay modes produces a surplus charged track they can be efficiently dealt with by an isolation technique. Once a signal candidate has been constructed, the other tracks in the event that are close to the B decay-vertex are then examined and a BDT is used to give a probability that these nearby tracks can be associated with the signal candidate decay-vertex. If the candidate is truly signal, there should be few other tracks that can be associated with it and the BDT should classify them with a low probability. On the other hand, the extra track(s) from a partially reconstructed decay will give a high probability of association if such tracks are found. The algorithm returns the BDT probabilities for the four tracks most likely to have come from the B vertex. These four probabilities are themselves combined into a single BDT classifier, known as the charged isolation BDT. This BDT is trained on simulation to discriminate signal from $B^+ \rightarrow \bar{A}_c^- p \mu^+ \nu_\mu$, which is expected to be the largest decay mode with extra charged tracks. The efficacy of this BDT in reducing such background is shown in Fig. 1.

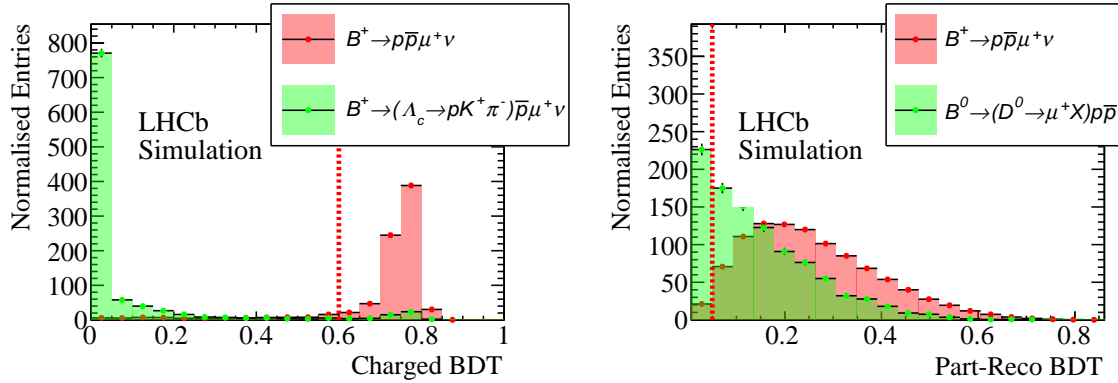


Figure 1: The result of training the (left) charged isolation BDT and the (right) part-reco BDT on the right. The chosen cut values are indicated by the red line. For some events there are no additional tracks near the B -decay vertex; these events are accepted and do not appear in the charged BDT output.

128 For those partially reconstructed final states with only extraneous neutral particles,
 129 additional suppression is achieved by considering the kinematics of the decays. A further
 130 BDT, the so called part-reco BDT, considers 11 variables: the impact parameter signif-
 131 icance of the three daughter tracks, the $p\bar{p}$ pair and the B^+ candidate with respect to
 132 the PV; the impact parameters of the tracks with respect to the fitted B^+ decay vertex;
 133 the χ^2 of the B^+ vertex fit; the angle between the B^+ candidate momentum and flight
 134 distance vectors; and the difference between the p and \bar{p} momenta. The part-reco BDT is
 135 trained on simulation in order to discriminate signal from a mixture of all the considered
 136 background modes. The result of this training is shown in Fig. 1

137 An additional background arises from particles that are misidentified as protons
 138 (misID). The particle identification requirements on the proton tracks are therefore further
 139 tightened relative to those from earlier. The background due to the muon being another
 140 misidentified particle is considered and is reduced to a negligible amount with only a loose
 141 particle identification cut.

142 In addition to the two BDTs and proton identification criteria, one further quantity is
 143 considered: the uncertainty on the corrected mass of the candidate. This is calculated from
 144 the estimated uncertainties on the positions of the B^+ primary and secondary vertices,
 145 and the momenta of the tracks. Selecting lower values of the corrected-mass uncertainty
 146 produces a sharper peak for the signal mode in the corrected mass variable, which will
 147 aid the discrimination of the signal from background in the fit to determine the yield.
 148 Therefore in total the selection uses five quantities (two BDTs, the proton PID, the muon
 149 PID and the corrected-mass error). In order to ascertain the optimal cut point, a five
 150 dimensional grid search is performed using pseudo-experiments. Datasets are generated
 151 from the simulation samples with the expected proportions of each background. The
 152 expected signal amount is taken from the central value of the $B^+ \rightarrow p\bar{p}e^+\nu_e$ branching
 153 fraction reported by Belle [8]. For the backgrounds, the current averages for the branching
 154 fractions are used if they have been measured. For those backgrounds that have not
 155 been measured their branching fractions are estimated relative to that expected for the
 156 signal, accounting for different CKM factors and the available phase-space. For each set
 157 of cuts in the grid the expected relative uncertainty on the signal yield is found by a fit

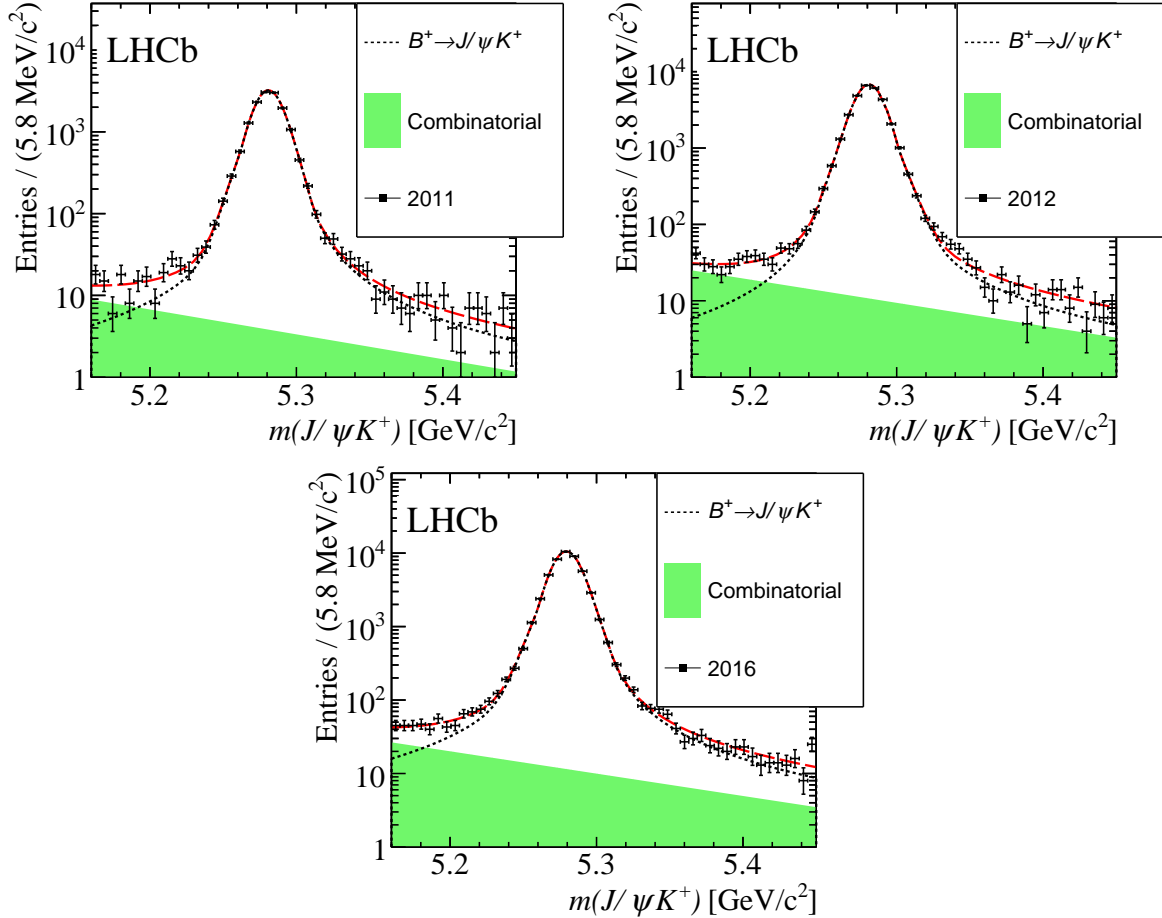


Figure 2: The $m(J/\psi K^+)$ distribution with the fit result shown for the (top left) 2011 data, (top right) 2012 and (bottom) 2016.

158 to the simulated data. These fits are not binned in $m(p\bar{p})$ but take the entire sample
 159 together. The set of cuts that produces the smallest relative uncertainty on the signal
 160 yield is chosen.

161 4 Signal and normalisation yields

162 The yields of signal and normalisation are ascertained with unbinned, extended, maximum-
 163 likelihood fits. In the case of the normalisation mode, the invariant mass distribution of
 164 the $J/\psi K^+$ candidates is fitted. The 2011, 2012 and 2016 datasets are fitted separately
 165 and then the yields combined. The fits are shown in Fig. 2.

166 For the signal mode, the corrected mass is fitted. The distribution of this variable
 167 peaks at the true B^+ rest mass for candidates where one particle with no mass is not
 168 reconstructed. On the other hand, candidates from partially reconstructed decays that are
 169 missing one or more massive particles in addition to the neutrino have wide distributions
 170 concentrated at lower corrected mass values. The Run 1 and 2016 data are combined and
 171 fitted together.

172 For the signal component and contributions from partially reconstructed decays the
 173 shapes are fixed from the simulation. The shape of the proton misID comes from a

174 separate independent data sample in which the particle identification requirements on one
 175 of the protons have been removed. Using this data sample the expected number of the
 176 proton misID candidates can be estimated and a Gaussian constraint is applied to the
 177 yield in the fit. A final background due to random combinations of protons and muons,
 178 referred to as the combinatorial background, is included in the fit. A sample of data for
 179 which the B^+ decay vertex quality selection has been reversed is used to estimate the
 180 shape of this background. The form of the signal probability density function (PDF) is
 181 parameterised by the sum of four bifurcated Gaussian functions with a shared mean. All
 182 of the background PDFs are accounted for with kernel density estimation [34].

183 The yields of the signal, proton misID, combinatorial and total partially reconstructed
 184 decays are determined by the fit, as are the relative fractions of each partially reconstructed
 185 mode. All of the fit parameters are free with the exception of the misID yield which is
 186 constrained.

187 The fit in each $m(p\bar{p})$ bin is performed independently. The m_{corr} distributions in
 188 each bin and the resulting fits are shown in Fig. 3. In each bin the fits are validated
 189 with pseudo-experiments. An ensemble of 10^5 datasets are generated and fitted with the
 190 component yields taken from the fits to data. Some small biases on the signal yield are
 191 found and these are considered as a source of systematic uncertainty.

192 5 Efficiency

193 The efficiencies for the signal and normalisation modes to be reconstructed and selected
 194 are both assessed with simulation. Further corrections are applied to account for known
 195 differences between data and simulation in the track reconstruction efficiency [35] and
 196 the efficiency of the hardware trigger [36]. The efficiency of the particle identification
 197 requirements on each track is evaluated with data [37] and applied to the simulation.

198 The binning in $m(p\bar{p})$ reduces the dependence on the model of the B^+ decay when
 199 calculating the efficiency of the signal mode. However, as the selection cuts on kinematic
 200 quantities of the candidates there is still some residual dependence on the physics of the
 201 decay. The simulation is therefore re-weighted to represent the pQCD model of Ref. [9]
 202 as the current best estimate of how the decay proceeds. This weighting corrects the
 203 distribution of the invariant mass of the di-lepton system (q^2). The variation of the
 204 parameters of this model is considered as a source of systematic uncertainty.

205 The ratio of selection efficiencies between the signal and normalisation in each bin of
 206 $m(p\bar{p})$ is shown in Table 1. These efficiencies are presented separately for the Run 1 and
 207 2016. They are combined to form an overall efficiency ratio, accounting for the difference
 208 in sample sizes between Run 1 and 2016.

209 6 Systematic uncertainties

210 The systematic uncertainties can be split into two categories: those that affect the
 211 calculation of the ratio of efficiencies of the signal and normalisation modes, and those
 212 that may change the determination of the signal yield in the fit. For the former, each of
 213 the corrections to the simulation contributes a source of uncertainty both from the limited
 214 sizes of the samples used to derive the corrections and from the method of deriving them.
 215 An alternative method to correct the distributions of p and p_T of the B^+ is used and the

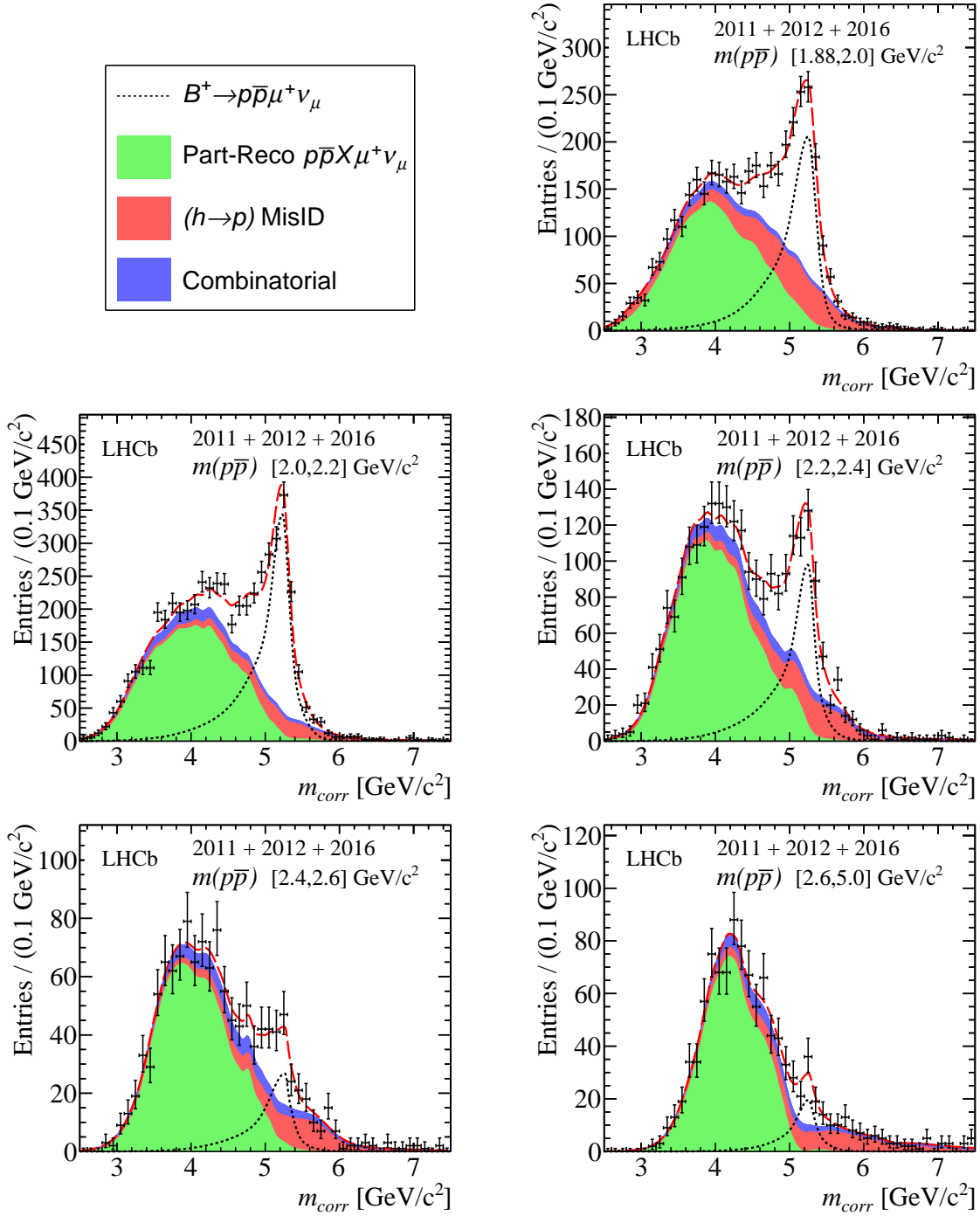


Figure 3: The distributions of m_{corr} in each $m(p\bar{p})$ bin with the fit results shown.

Table 1: Relative efficiencies for the Run 1 and 2016 and the weighted combination of both.

$m(p\bar{p})_i$ [GeV/c ²]	$\frac{\epsilon(B \rightarrow p\bar{p}\mu\nu)_{m(p\bar{p})}}{\epsilon(B \rightarrow J/\psi K)}$		
	Run 1	2016	Run 1&2016
1.87 – 2.0	0.369 ± 0.022	0.567 ± 0.032	0.477 ± 0.024
2.0 – 2.2	0.366 ± 0.020	0.513 ± 0.027	0.446 ± 0.021
2.2 – 2.4	0.358 ± 0.020	0.504 ± 0.026	0.438 ± 0.021
2.4 – 2.6	0.361 ± 0.021	0.519 ± 0.027	0.447 ± 0.021
2.6 – 5.0	0.350 ± 0.020	0.489 ± 0.024	0.426 ± 0.020

216 relative efficiencies recalculated. An additional uncertainty due to any residual differences
 217 between data and simulation is determined using the $B^+ \rightarrow J/\psi K^+$ mode. The difference
 218 in efficiency when cutting on the two BDTs and corrected mass error variable is compared
 219 between data and simulation for the mode.

220 To account for the uncertainty in the correction of the simulation for the reconstruction
 221 efficiency of each track, the applied weights are varied within their uncertainties and again
 222 the relative efficiencies recalculated. Similarly an uncertainty is assessed for the particle
 223 identification weights applied to each track. The uncertainty due to the limited simulation
 224 sample sizes used to calculate the efficiencies is also included.

225 A further uncertainty is due to the physics model that the simulation is weighted to
 226 represent. The model affects the kinematic distributions of the daughter tracks which
 227 feeds into the efficiency calculation as these distributions are cut on. Due to the unproven
 228 nature of the model, a conservative uncertainty is taken. New sets of weights for the
 229 simulation are created that sample extreme variations of the model parameters ($\pm 5\sigma$) and
 230 for each variation the efficiency is recalculated. Despite this extreme test the systematic
 231 due to the physics model is not dominant, which reflects the flat selection efficiency over
 232 the kinematic ranges in which the daughter tracks lie within each bin of $m(p\bar{p})$.

233 In the corrected mass fit uncertainties arise from potential variations in the shapes of the
 234 components. This variation is assessed with pseudo-experiments. Datasets are generated
 235 with the nominal fit model and then fitted with the nominal model and an alternative.
 236 The width of the distribution of differences between the nominal and alternative fits gives
 237 the uncertainty. For those components that rely on kernel density estimators, a systematic
 238 is assessed for the choice of smoothing parameter by varying it. The uncertainty due to
 239 the choice of model for the signal shape is found by replacing the nominal PDF with one
 240 constructed with kernel density estimators. The uncertainty due to the limited statistics
 241 of the simulation samples is determined by generating new simulation from the nominal fit
 242 PDFs with the same statistics and making alternative PDFs with those samples. For the
 243 shape of the combinatorial background component an alternative data sample is trialled
 244 which requires the two protons to be of the same charge.

245 A summary of the systematic uncertainties is presented in Table 2. They are given as
 246 relative uncertainties on the branching fraction with the combination accounting for the
 247 correlation of the uncertainties between the two datasets.

Table 2: A summary of the systematic uncertainties on the differential branching fractions. The particle identification and tracking efficiency systematics are assumed to be 100% correlated between Run 1 and 2016.

Source	Range of relative uncertainties on \mathcal{B} [%]
Kinematic reweighting	0.39 – 0.56
Simulation statistics	2.98 – 3.63
Tracking efficiency	2.74– 2.74
Physics model	0.01 – 0.05
Particle identification	0.68 – 1.67
Data-simulation agreement	0.40
Run 1 and 2016 combination	1.63 – 2.06
Kernel smoothing	0.02 – 7.90
Signal model	0.59 – 9.87
misID model	0.13 – 13.46
Simulation statistics	0.02 – 5.16
Combinatorial model	0.90 – 8.51
Fit bias	0.13 – 7.80
Total systematic uncertainty	5.20 – 20.37
Total statistical uncertainty	5.54 – 29.64

7 Results

248

249 The fitted yields for the signal mode are presented in Table 3. The extracted yields of
 250 the normalisation channel are $(1.493 \pm 0.026) \times 10^4$ for 2011, $(3.138 \pm 0.019) \times 10^4$ for
 251 2012 and $(4.927 \pm 0.025) \times 10^4$ for 2016. Combining these with the efficiency ratios from
 252 Section 5, the differential branching fraction in each $m(p\bar{p})$ bin is calculated, relative to
 253 the branching fraction of the normalisation mode. The results are presented in the third
 254 column of Table 3. The relative differential branching fractions are then summed over the
 255 bins, with the correlation of the systematic uncertainties between the bins accounted for,
 256 to give the total relative branching fraction of

$$\frac{\mathcal{B}(B^+ \rightarrow p\bar{p}\mu^+\nu_\mu)}{\mathcal{B}(B^+ \rightarrow (J/\psi \rightarrow \mu^+\mu^-)K^+)} = (8.75 \pm 0.39 \pm 0.35) \times 10^{-2},$$

257 where the first uncertainty is statistical and the second systematic. Multiplying this by
 258 the current average of the normalisation branching fraction [13] leads to

$$\mathcal{B}(B^+ \rightarrow p\bar{p}\mu^+\nu_\mu) = (5.27_{-0.24}^{+0.23} \pm 0.21 \pm 0.15) \times 10^{-6},$$

259 where the third uncertainty is from the normalisation branching fraction. Finally, the
 260 absolute differential branching fraction as a function of $m(p\bar{p})$ is shown in Fig. 4, where
 261 the indicated uncertainties include statistical, systematic and normalisation uncertainty
 262 contributions. As expected from the theory model and the analogous hadronic decays,
 263 the differential distribution peaks at a very low value and falls off sharply. The measured
 264 total branching fraction agrees with the previous measurement from Belle and represents
 265 the first observation of the $B^+ \rightarrow p\bar{p}\mu^+\nu_\mu$ decay mode.

Table 3: Table of the number of observed $B^+ \rightarrow p\bar{p}\mu^+\nu_\mu$ candidates in each bin of $p\bar{p}$ mass with the associated statistical uncertainty.

$p\bar{p}$ Mass range [GeV/c ²]	Signal Yield	$d\mathcal{B}(B^+ \rightarrow p\bar{p}\mu^+\nu_\mu)/dm(p\bar{p})$ [$\times 10^{-6}$ GeV ⁻¹ c ²]
1.87 – 2.0	1208 ⁺¹¹¹ ₋₁₁₀	12.86 ^{+1.18} _{-1.17} \pm 0.69 \pm 0.38
2.0 – 2.2	1826 ⁺⁹⁷ ₋₁₀₅	12.88 ^{+0.69} _{-0.74} \pm 0.68 \pm 0.38
2.2 – 2.4	526 ⁺⁶⁷ ₋₆₄	3.78 ^{+0.48} _{-0.46} \pm 0.24 \pm 0.11
2.4 – 2.6	148 ⁺⁴⁰ ₋₃₅	1.038 ^{+0.279} _{-0.248} \pm 0.162 \pm 0.030
2.6 – 5.0	88 ⁺²⁶ ₋₂₆	0.0542 ^{+0.0163} _{-0.0160} \pm 0.0113 \pm 0.0016

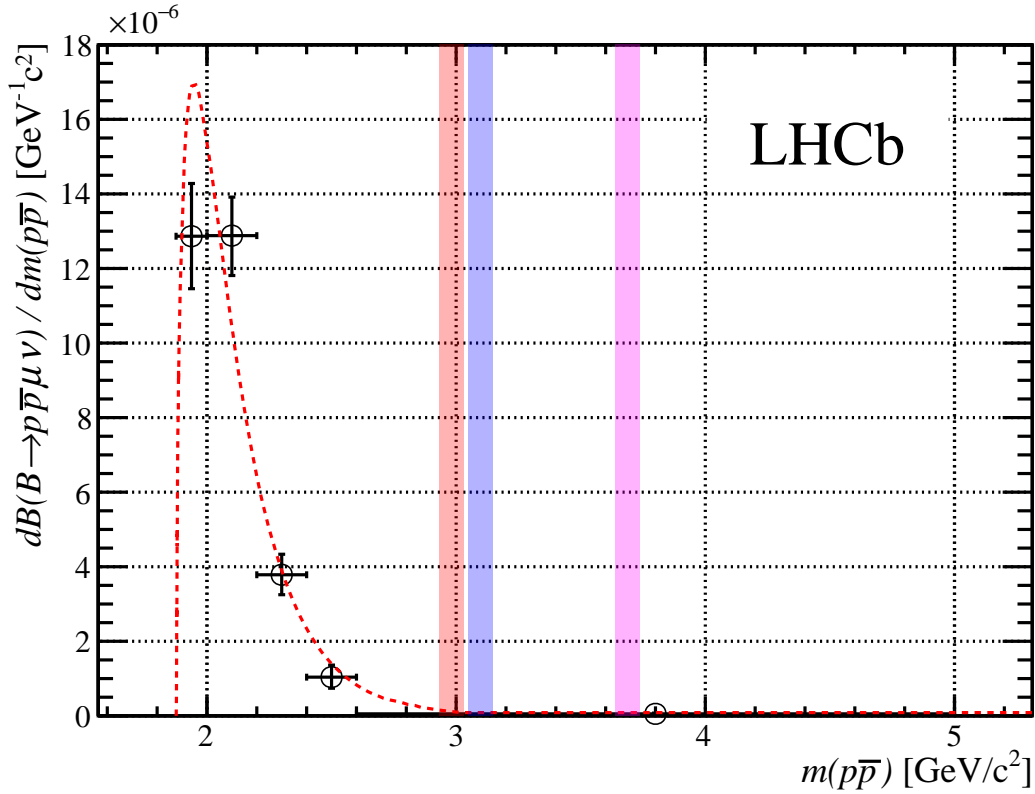


Figure 4: Differential branching fraction as a function of $p\bar{p}$ mass. The (left) red band indicates the $\eta_c \rightarrow p\bar{p}$ veto and (middle) blue band indicates the $J/\psi \rightarrow p\bar{p}$ veto. The $\psi(2S)$ veto is the (right) pink band. The red dashed line indicates the pQCD model normalised to the observed branching fraction [9].

266 Acknowledgements

267 We express our gratitude to our colleagues in the CERN accelerator departments for the
268 excellent performance of the LHC. We thank the technical and administrative staff at the
269 LHCb institutes. We acknowledge support from CERN and from the national agencies:
270 CAPES, CNPq, FAPERJ and FINEP (Brazil); MOST and NSFC (China); CNRS/IN2P3
271 (France); BMBF, DFG and MPG (Germany); INFN (Italy); NWO (Netherlands); MNiSW
272 and NCN (Poland); MEN/IFA (Romania); MSHE (Russia); MinECo (Spain); SNSF and
273 SER (Switzerland); NASU (Ukraine); STFC (United Kingdom); DOE NP and NSF (USA).
274 We acknowledge the computing resources that are provided by CERN, IN2P3 (France),
275 KIT and DESY (Germany), INFN (Italy), SURF (Netherlands), PIC (Spain), GridPP
276 (United Kingdom), RRCKI and Yandex LLC (Russia), CSCS (Switzerland), IFIN-HH
277 (Romania), CBPF (Brazil), PL-GRID (Poland) and OSC (USA). We are indebted to
278 the communities behind the multiple open-source software packages on which we depend.
279 Individual groups or members have received support from AvH Foundation (Germany);
280 EPLANET, Marie Skłodowska-Curie Actions and ERC (European Union); ANR, Labex
281 P2IO and OCEVU, and Région Auvergne-Rhône-Alpes (France); Key Research Program
282 of Frontier Sciences of CAS, CAS PIFI, and the Thousand Talents Program (China);
283 RFBR, RSF and Yandex LLC (Russia); GVA, XuntaGal and GENCAT (Spain); the
284 Royal Society and the Leverhulme Trust (United Kingdom).

8 Supplementary material for LHCb-PAPER-20XX-YYY

Figure 5: Correlations in the uncertainties between bins of $p\bar{p}$ mass.

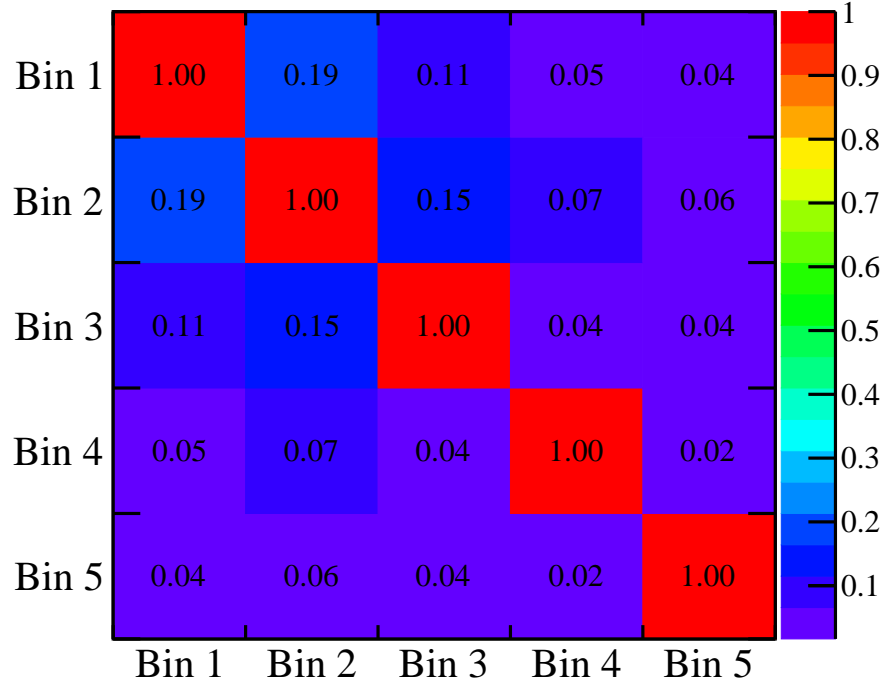


Table 4: Covariance matrix for bins of $p\bar{p}$ mass.

[GeV ⁻² c ⁴]	Bin 1	Bin 2	Bin 3	Bin 4	Bin 5
Bin 1	1.991e-12	2.800e-13	8.532e-14	2.307e-14	1.249e-15
Bin 2	2.800e-13	1.106e-12	8.332e-14	2.264e-14	1.211e-15
Bin 3	8.532e-14	8.332e-14	2.945e-13	6.905e-15	3.771e-16
Bin 4	2.307e-14	2.264e-14	6.905e-15	9.638e-14	1.011e-16
Bin 5	1.249e-15	1.211e-15	3.771e-16	1.011e-16	3.901e-16

References

- 287
- 288 [1] LHCb collaboration, R. Aaij *et al.*, *Measurement of the ratio of the $\mathcal{B}(B^0 \rightarrow D^{*-} \tau^+ \nu_\tau)$*
289 *and $\mathcal{B}(B^0 \rightarrow D^{*-} \mu^+ \nu_\mu)$ branching fractions using three-prong τ -lepton decays*, Phys. Rev. Lett. **120** (2018) 171802, [arXiv:1708.08856](#).
290
- 291 [2] LHCb collaboration, R. Aaij *et al.*, *Measurement of the ratio of branching frac-*
292 *tions $\mathcal{B}(\bar{B}^0 \rightarrow D^{*+} \tau^- \bar{\nu}_\tau)/\mathcal{B}(\bar{B}^0 \rightarrow D^{*+} \mu^- \bar{\nu}_\mu)$* , Phys. Rev. Lett. **115** (2015) 111803,
293 *Publisher's Note* *ibid.* **115** (2015) 159901, [arXiv:1506.08614](#).
- 294 [3] Belle, A. Abdesselam *et al.*, *Measurement of $\mathcal{R}(D)$ and $\mathcal{R}(D^*)$ with a semileptonic*
295 *tagging method*, [arXiv:1904.08794](#).
- 296 [4] Belle, S. Hirose *et al.*, *Measurement of the τ lepton polarization and $R(D^*)$ in the*
297 *decay $\bar{B} \rightarrow D^* \tau^- \bar{\nu}_\tau$* , Phys. Rev. Lett. **118** (2017) 211801, [arXiv:1612.00529](#).
- 298 [5] Belle, M. Huschle *et al.*, *Measurement of the branching ratio of $\bar{B} \rightarrow D^{(*)} \tau^- \bar{\nu}_\tau$*
299 *relative to $\bar{B} \rightarrow D^{(*)} \ell^- \bar{\nu}_\ell$ decays with hadronic tagging at Belle*, Phys. Rev. **D92**
300 (2015) 072014, [arXiv:1507.03233](#).
- 301 [6] BaBar, J. P. Lees *et al.*, *Evidence for an excess of $\bar{B} \rightarrow D^{(*)} \tau^- \bar{\nu}_\tau$ decays*, Phys. Rev.
302 Lett. **109** (2012) 101802, [arXiv:1205.5442](#).
- 303 [7] Heavy Flavor Averaging Group, Y. Amhis *et al.*, *Averages of b -hadron, c -*
304 *hadron, and τ -lepton properties as of summer 2016*, Eur. Phys. J. **C77**
305 (2017) 895, [arXiv:1612.07233](#), updated results and plots available at
306 <https://hflav.web.cern.ch>.
- 307 [8] Belle, K.-J. Tien *et al.*, *Evidence for semileptonic $B^- \rightarrow p \bar{p} \ell^- \bar{\nu}_\ell$ decays*, Phys. Rev.
308 **D89** (2014) 011101, [arXiv:1306.3353](#).
- 309 [9] C. Q. Geng and Y. K. Hsiao, *Semileptonic $B^- \rightarrow p \bar{p} \ell^- \bar{\nu}_\ell$ decays*, Phys. Lett. **B704**
310 (2011) 495, [arXiv:1107.0801](#).
- 311 [10] C. Q. Geng and Y. K. Hsiao, *Angular distributions in three-body baryonic b decays*,
312 Phys. Rev. D **74** (2006) 094023.
- 313 [11] C.-H. Chen, H.-Y. Cheng, C. Q. Geng, and Y. K. Hsiao, *Charmful three-body baryonic*
314 *b decays*, Phys. Rev. D **78** (2008) 054016.
- 315 [12] LHCb collaboration, R. Aaij *et al.*, *First observation of the rare purely baryonic decay*
316 *$B^0 \rightarrow p \bar{p}$* , Phys. Rev. Lett. **119** (2017) 232001, [arXiv:1709.01156](#).
- 317 [13] Particle Data Group, M. Tanabashi *et al.*, *Review of particle physics*, Phys. Rev.
318 **D98** (2018) 030001.
- 319 [14] BaBar, B. Aubert *et al.*, *Evidence for the $B^0 \rightarrow p \bar{p} K^{*0}$ and $B^+ \rightarrow p \bar{p} \eta(c)$*
320 *K^{*+} decays and Study of the Decay Dynamics of B Meson Decays into p anti- p h*
321 *final states*, Phys. Rev. **D76** (2007) 092004, [arXiv:0707.1648](#).

- 322 [15] BaBar, B. Aubert *et al.*, *Measurements of the Decays $B^0 \rightarrow \bar{D}^0 p \bar{p}$, $B^0 \rightarrow \bar{D}^* 0 p \bar{p}$, $B^0 \rightarrow D^- p \bar{p} \pi^+$, and $B^0 \rightarrow D^{*-} p \bar{p} \pi^+$* , Phys. Rev. **D74** (2006) 051101,
323 arXiv:hep-ex/0607039.
324
- 325 [16] Belle, M. Z. Wang *et al.*, *Observation of $B^+ \rightarrow p \text{ anti-}p \pi^+$, $B^0 \rightarrow p \text{ anti-}p K^0$, and
326 $B^+ \rightarrow p \text{ anti-}p K^{*+}$* , Phys. Rev. Lett. **92** (2004) 131801, arXiv:hep-ex/0310018.
- 327 [17] SLD, K. Abe *et al.*, *A Measurement of $R(b)$ using a vertex mass tag*, Phys. Rev. Lett.
328 **80** (1998) 660, arXiv:hep-ex/9708015.
- 329 [18] LHCb, A. A. Alves, Jr. *et al.*, *The LHCb Detector at the LHC*, JINST **3** (2008)
330 S08005.
- 331 [19] LHCb, R. Aaij *et al.*, *LHCb Detector Performance*, Int. J. Mod. Phys. **A30** (2015)
332 1530022, arXiv:1412.6352.
- 333 [20] R. Aaij *et al.*, *Performance of the LHCb Vertex Locator*, JINST **9** (2014) P09007,
334 arXiv:1405.7808.
- 335 [21] LHCb Outer Tracker Group, R. Arink *et al.*, *Performance of the LHCb Outer Tracker*,
336 JINST **9** (2014) P01002, arXiv:1311.3893.
- 337 [22] LHCb Outer Tracker Group, P. d'Argent *et al.*, *Improved performance of the LHCb
338 Outer Tracker in LHC Run 2*, JINST **12** (2017) P11016, arXiv:1708.00819.
- 339 [23] LHCb RICH Group, M. Adinolfi *et al.*, *Performance of the LHCb RICH detector at
340 the LHC*, Eur. Phys. J. **C73** (2013) 2431, arXiv:1211.6759.
- 341 [24] A. A. Alves, Jr. *et al.*, *Performance of the LHCb muon system*, JINST **8** (2013)
342 P02022, arXiv:1211.1346.
- 343 [25] R. Aaij *et al.*, *The LHCb Trigger and its Performance in 2011*, JINST **8** (2013)
344 P04022, arXiv:1211.3055.
- 345 [26] V. V. Gligorov and M. Williams, *Efficient, reliable and fast high-level triggering using
346 a bonsai boosted decision tree*, JINST **8** (2013) P02013, arXiv:1210.6861.
- 347 [27] T. Sjöstrand, S. Mrenna, and P. Skands, *PYTHIA 6.4 physics and manual*, JHEP
348 **05** (2006) 026, arXiv:hep-ph/0603175; T. Sjöstrand, S. Mrenna, and P. Skands,
349 *A brief introduction to PYTHIA 8.1*, Comput. Phys. Commun. **178** (2008) 852,
350 arXiv:0710.3820.
- 351 [28] I. Belyaev *et al.*, *Handling of the generation of primary events in Gauss, the LHCb
352 simulation framework*, J. Phys. Conf. Ser. **331** (2011) 032047.
- 353 [29] D. J. Lange, *The EvtGen particle decay simulation package*, Nucl. Instrum. Meth.
354 **A462** (2001) 152.
- 355 [30] P. Golonka and Z. Was, *PHOTOS Monte Carlo: A precision tool for QED corrections
356 in Z and W decays*, Eur. Phys. J. **C45** (2006) 97, arXiv:hep-ph/0506026.

- 357 [31] Geant4 collaboration, J. Allison *et al.*, *Geant4 developments and applications*, IEEE
358 Trans. Nucl. Sci. **53** (2006) 270; Geant4 collaboration, S. Agostinelli *et al.*, *Geant4:*
359 *A simulation toolkit*, Nucl. Instrum. Meth. **A506** (2003) 250.
- 360 [32] M. Clemencic *et al.*, *The LHCb simulation application, Gauss: Design, evolution and*
361 *experience*, J. Phys. Conf. Ser. **331** (2011) 032023.
- 362 [33] A. Rogozhnikov, *Reweighting with Boosted Decision Trees*, J. Phys. Conf. Ser. **762**
363 (2016) , [arXiv:1608.05806](https://arxiv.org/abs/1608.05806), https://github.com/arogozhnikov/hep_ml.
- 364 [34] K. S. Cranmer, *Kernel estimation in high-energy physics*, Comput. Phys. Commun.
365 **136** (2001) 198, [arXiv:hep-ex/0011057](https://arxiv.org/abs/hep-ex/0011057).
- 366 [35] T. L. collaboration, *Measurement of the track reconstruction efficiency at LHCb*,
367 Journal of Instrumentation **10** (2015) P02007.
- 368 [36] S. Tolk, J. Albrecht, F. Dettori, and A. Pellegrino, *Data driven trigger efficiency*
369 *determination at LHCb*, LHCb-PUB-2014-039, 2014.
- 370 [37] L. Anderlini *et al.*, *The PIDCalib package*, LHCb-PUB-2016-021, 2016.

LHCb collaboration

371 A. N. Other¹.

372 ¹*University of nowhere*